applied system innovation

MDPI

Article

Chaos Synchronization in Visible Light Communications with Variable Delays Induced by Multipath Fading

Pep Canyelles-Pericas [1,*,†], Paul Anthony Haigh [2,†], Zabih Ghassemlooy [1], Andrew Burton [1], Xuewu Dai [1], Tran The Son [3], Hoa Le-Minh [1], Richard Binns [1] and Krishna Busawon [1]

1 Faculty of Engineering and Environment, University of Northumbria at Newcastle, Ellison Building, Newcastle upon Tyne NE1 8ST, UK; z.ghassemlooy@northumbria.ac.uk (Z.G.); andrew2.burton@northumbria.ac.uk (A.B.); xuewu.dai@northumbria.ac.uk (X.D.); hoa.le-minh@northumbria.ac.uk (H.L.-M.); richard.binns@northumbria.ac.uk (R.B.); krishna.busawon@northumbria.ac.uk (K.B.)

2 Institute of Communications and Information Systems, University College London, Gower Street, London WC1E 6BT, UK; p.haigh@ucl.ac.uk

3 Faculty of Computer Sciences, Korea-Vietnam Friendship IT College, Tran Dai Nghia Street, Da Nang City 236, Vietnam; trantheson@mic.gov.vn

* Correspondence: pep.canyelles-pericas@northumbria.ac.uk; Tel.: +44-0-79-3859-2794

† These authors contributed equally to this work.

Received: 10 October 2018; Accepted: 5 November 2018; Published: 9 November 2018

Abstract: Visible Light Communication (VLC) uses light-emitting diodes to provide wireless connectivity in public environments. Transmission security in this emerging channel is not trivial. Chaotic modulation techniques can provide encryption directly in the physical layer based on the random-alike evolution and strong synchronization prospect given by deterministic chaos. In secure chaotic inclusion or embedding methods, continuous-time chaos oscillator models need to be synchronized via a coupling carrier. Here we present a first numerical simulation study for the impact of the variable delays induced by line-of-sight and non-line-of-sight multipath fading in complete chaotic synchronization. More precisely, we analyze a chaotic Colpitts oscillator that is simultaneously transmitting the carrier to several mobile receivers via nine spotlights. Such induced delays depend on both the receiver position and the carrier frequency, influencing the complete synchronization required in modulation via chaotic inclusion. Correlation values for several receiver positions and carrier frequencies are presented, examining the progressive emergence of the multipath effect and its impact on chaotic synchronization. We show that, for the chaotic oscillator and coupling applied in the defined room settings, complete chaotic synchronization can be achieved and that it is robust up to the tens of MHz region.

Keywords: visible light communication; chaotic communication; multipath channels; nonlinear systems; network security; chaos synchronization

1. Introduction

Chaos communications exploit the properties displayed by chaotic oscillators to provide security in data transmission at the physical layer [1]. Low-order chaotic systems are bounded in values but aperiodic in nature. These are theoretically composed by an infinite amount of frequencies and, although being deterministic, they present an extreme sensitivity with respect to the initial conditions that makes long term prediction impossible.

Despite the sensitivity towards the starting point, chaotic oscillators can be set to synchronize in several modes, provided that adequate coupling mechanisms are implemented [2,3]. This pseudorandom-evolution and synchrony prospects associate very well with both the standard cryptographic and data transmission requirements [4], thus paving the way for secure, chaos-based, communications. There are broadly two main categories of chaos synchronization schemes: one is based in continuous time models (e.g., dynamical systems), such as ordinary differential equations. The other group corresponds to discrete models such as chaotic maps. To synchronize the first group, one needs to transmit a chaotic signal carrier continuously over time, which is affected by channel effects such as multipath. The discrete group can be set to synchronize with the transmission of a secret key only, but with less cryptographic potential [1].

Visible light communication (VLC) is an emerging free space optical communication method built upon intensity modulation of light-emitting diodes (LEDs). LEDs, fabricated with p-n junction technology, produce light based on the principle of electroluminescence, where photonic emission takes place in response to an electric field. Their fundamental operation allows LEDs to be switched on and off beyond millions of times per second, far too fast for the human eye to realize flickering, enabling binary transmission of information in combination with adequate photodetectors. Accordingly, VLC allows high data rates in the Gb/s region [5,6]. In fact, most related research has focused on increasing the data rates or implementation of full duplex links (VLC-infrared, VLC-WiFi, and fully VLC). There are many VLC applications including data communications, indoor localization positioning and multi-user access environments [7–13]. In effect, VLC is a complementary technology to Wi-Fi for fourth and fifth generation (4G/5G) wireless systems. This is particularly useful as Wi-Fi presents difficulties in providing multi-user connectivity. Additionally, LEDs are becoming the first choice as lighting fixtures for indoor environments due to their high energy efficiency, longer life expectancy, fast switching capability, and comparatively low costs. Moreover, advancements in thin film technology allow the fabrication of organic LEDs in large panels, widening its application fields [14]. Their implementation is going beyond indoor lighting as they are being deployed in car lights, streetlights, stand-by pilots, and so on. Consequently, LEDs are potential data transmitters (Txs) in a range of different environments, including car-to-car communications [15], wireless sensor networks, or the Internet of Things (IoT) [16]. In VLC based wireless systems, to avoid blocking and shadowing, hence ensuring 100% link availability, Tx and receiver (Rx) arrays have been adopted to provide diversity, but at the cost of increased multipath induced delay spread that leads to reduced data rates (e.g., [17,18]).

In certain applications, such as indoor or outdoor public spaces, banking, manufacturing, medical, etc., the issue of data security is becoming extremely important. Typical cryptographic techniques used today utilize number theory principles, a branch of mathematics that studies the topology of numbers. While these methods have served well in the last decades, they seem to have their security compromised with the emergence of high-speed computing; capable to process large computation of data sets. Whereas in quantum key distribution (QKD) based protocols, which are popular in optical fiber networks [19], there is the need for a coherent light source (e.g., from laser sources) [20]. These schemes cannot be adopted in indoor VLC systems. Alternatively, the more recent approach of chaos, emerging from an interdisciplinary branch of mathematics, is a promising candidate. Thus, high security-based VLC links could be implemented based on chaos communications [21].

It should be noted, however, that not all chaotic cryptosystems proposed in the literature can be considered cryptographically robust by default [22,23]. Nonetheless, the chaotic inclusion (or embedding) method, which uses continuous-time chaotic models, is considered secure and implementable in practice [24]. For its practical implementation, chaotic inclusion requires total synchronization between the chaotic oscillators involved. In chaos theory terminology, this kind of synchronization is referred to as complete, total, or identical; defined as overall convergence between Tx and Rx over time under different initial conditions. That is, for a chaotic Tx $\dot{x}(t) = f(x(t))$ and a Rx $\dot{\hat{x}}(t) = f(\hat{x}(t))$, complete synchronization is achieved when $\lim_{t\to\infty} ||x(t) - \hat{x}(t)|| = 0$ for $x(0) \neq \hat{x}(0)$ [3].

Considering the high sensitivity of chaotic systems to the initial conditions, the prospect of achieving total synchrony is non-trivial, especially under the effect of wireless channel conditions [25,26].

The end purpose is to study the suitability of chaotic inclusion schemes in VLC. In the context of chaos synchronization, it is not clear that the coupling methodology, via a chaotic signal acting as a carrier, can handle the variable delay induced by the multipath effect. Furthermore, these delays vary depending on both the Rx position and the frequency of the carrier signal. As result, complete or total chaotic synchronization is a function of both factors.

In this way, this work finely analyzes the upraise and impact of multipath delays in chaotic synchronization while suggesting a region limit in the carrier frequency, progressively lifted with time normalization procedures. We study the degree of complete synchronization based on cross correlation coefficients for continuous-time Colpitts chaotic synchronization. In more detail, we investigate chaos synchronization in a multiple input single output (MISO) VLC for both line of sight (LOS) and non-LOS propagation schemes. The results presented are based on numerical simulation models.

The paper is structured as follows. Section 1 has introduced the problem statement. Section 2 provides a description of the working models for the Colpitts model employed with its related chaotic coupling mechanism in an ideal channel and the VLC multipath model implemented. Section 3 presents the numerical simulation results obtained. Finally, conclusions are drawn in Section 4.

2. Working Models

2.1. Colpitts Chaotic Synchronization

The Colpitts circuit is a classic harmonic oscillator, being one of the most widely used electronic designs for the development of harmonic data transmission for almost a century. Interestingly, in 1994 it was reported that a parametric set of circuit values creates chaotic dynamics [27]. The Colpitts circuit consists of a single bipolar junction transistor (BJT), which is biased in its active region [27,28]. A combination of inductor L, capacitance divider, and resistance R was used as a feedback network. Figure 1 shows a circuit schematic.

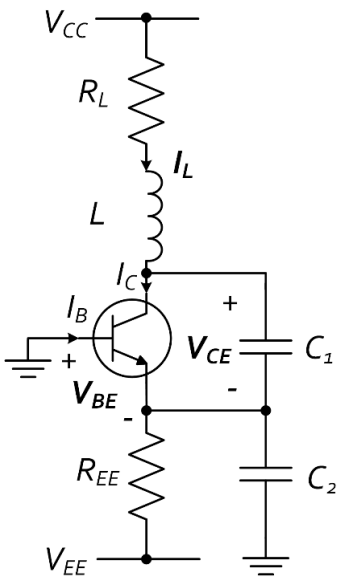

Figure 1. Colpitts circuit.

Based on the respective Kirchhoff analysis, the dynamics of the Colpitts oscillators with symmetrical feedback operated in the forward active and cut-off regions can be described by a system of three autonomous state equations given by:

$$\begin{cases} C_1 \frac{dV_{CE}(t)}{dt} = I_L(t) - I_C(t) \\ C_2 \frac{dV_{BE}(t)}{dt} = -\frac{V_{EE}+V_{BE}(t)}{R_{EE}} - I_L(t) - I_B(t) \\ L \frac{dI_L(t)}{dt} = V_{CC} - V_{CE}(t) + V_{BE}(t) - I_L(t)R_L \end{cases} \quad (1)$$

where V_{CC} and V_{EE} are the positive and negative power supply voltages, respectively. $V_{CE}(t)$ and $V_{BE}(t)$ are the collector-emitter voltage and the base-emitter voltage correspondingly and $I_L(t)$ is the current flowing through L. The Kirchhoff analysis also shows that both the base and collector currents $I_B(t)$ and $I_C(t)$, both depend on $V_{BE}(t)$. Let V_{TH} denote the transistor's voltage threshold and R_{ON} its corresponding internal resistance in the conducting mode, the BJT's switching between the cut-off and active modes result in the jump of the Colpitts dynamics. Finally, the term β is the forward current gain of the transistor. The switching law that represents the transistor behavior can be modelled as a two-segment piecewise linear function:

$$I_B(t) = \begin{cases} 0 & if\ V_{BE}(t) \leq V_{TH} \\ \frac{V_{BE}(t)-V_{TH}}{R_{ON}} & if\ V_{BE}(t) > V_{TH} \end{cases}, I_C(t) = \beta I_B(t), \quad (2)$$

In this study, we have adopted the circuit parameters described in [28], obtained from experimental setups. The parameters are given in Table 1. The single bipolar junction transistor employed is the model 2SC1740 with a cutoff frequency of 180 MHz, from which the operating values are extracted. The interested reader can refer to [28] for further detail.

Table 1. Colpitts circuit parameters.

Parameters	Values
C_1 (nF)	58
C_2 (nF)	58
L (µH)	100
R_L (Ω)	36
R_{EE} (Ω)	430
V_{CC} (V)	5
V_{EE} (V)	−5
R_{ON} (Ω)	375
β	230
V_{TH}	0.7

Figure 2 shows the voltage and current waveforms for all the states given in (1) when operating in chaotic mode, that is, when using the parameters given in Table 1. $V_{BE}(t)$ is highlighted since it represents the transmitted carrier signal, which is also used at the Rx to ensure coupling between both chaotic trajectories. Further detail is given in the upcoming paragraphs. As follows we show Colpitts chaotic attractor projection, obtained by plotting the states against each other, shown in Figure 3.

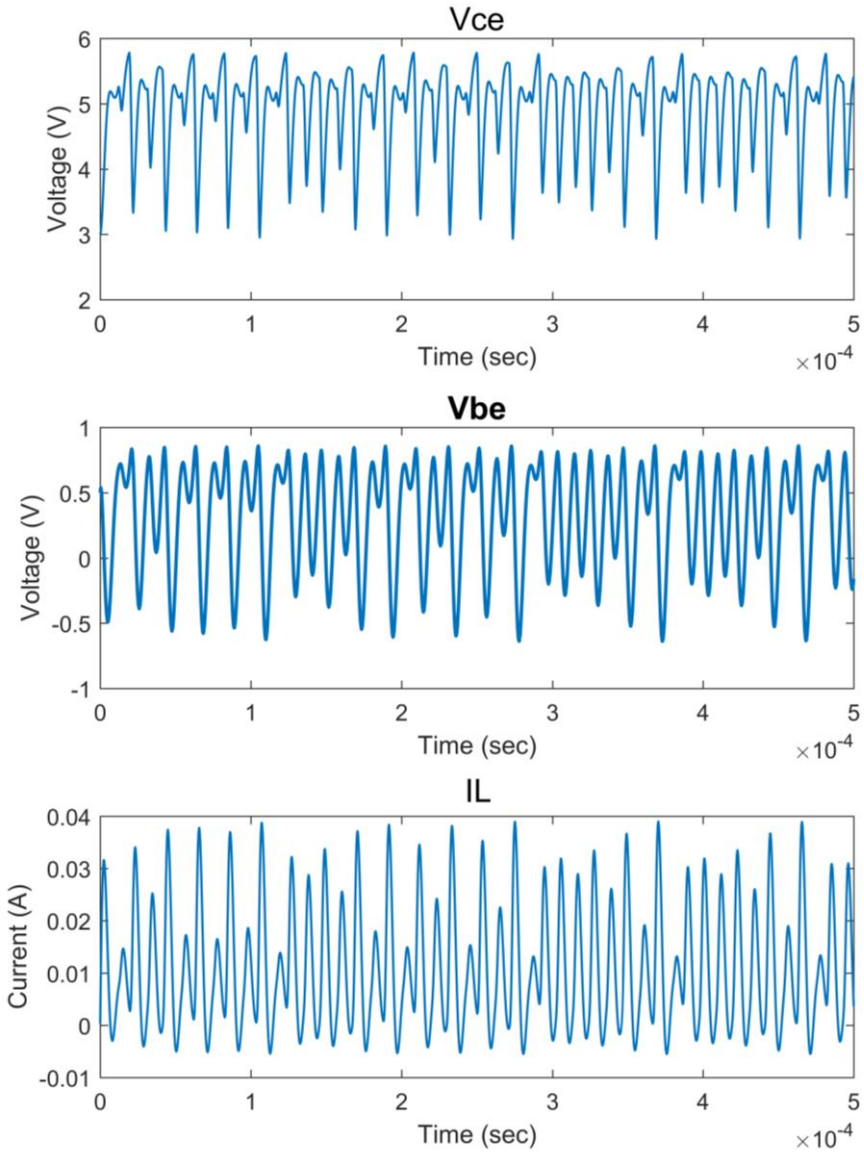

Figure 2. Colpitts chaotic time series.

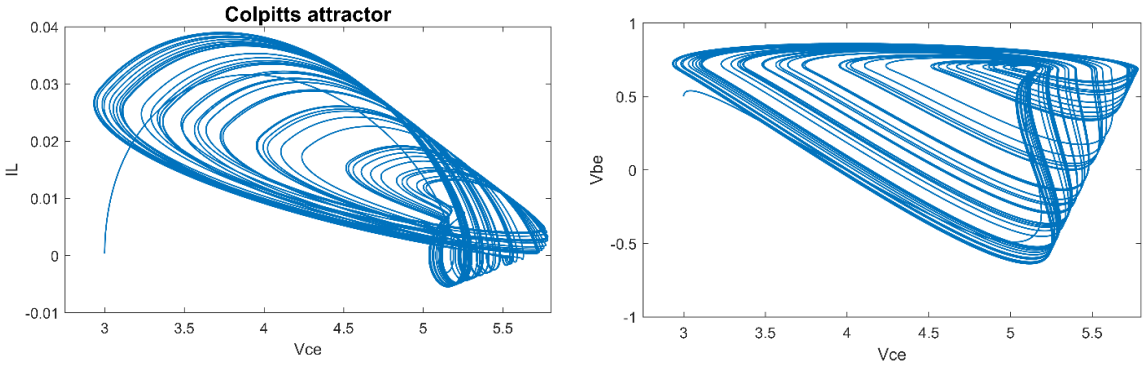

Figure 3. Colpitts attractor projections.

As an illustrative example, we show the chaotic synchronization method employed for an ideal channel. We assume that, both Tx and Rx have identical parameters except for the initial conditions, which are set at different values.

For this we use the identical (or complete) chaotic synchronization methodology proposed in [29], where $V_{BE\_TX}(t)$ (i.e., the chaotic carrier signal) replaces $V_{BE\_RX}(t)$ and directly dependent terms of $I_{B\_RX}(t)$ and $I_{C\_RX}(t)$ in the 1st and 3rd equations of (3). Note that, $V_{BE\_RX}(t)$ is left unchanged in the 2nd equation. More precisely, the Rx model is given by:

$$\begin{cases} C_1 \frac{dV_{CE\_RX}(t)}{dt} = I_{L\_RX}(t) - I_{C\_TX}(t)) \\ C_2 \frac{dV_{BE\_RX}(t)}{dt} = -\frac{V_{EE}+V_{BE\_RX}(t)}{R_{EE}} - I_{L\_RX}(t) - I_{B\_RX}(t) \\ L \frac{dI_{L\_RX}(t)}{dt} = V_{CC} - V_{CE\_RX}(t) + V_{BE\_TX}(t) - I_{L\_RX}(t)R_L \end{cases}, \quad (3)$$

Note that the Rx's piecewise linear function is identical to (2), and therefore omitted for clarity purposes. Using (1) and (3) we plot the simulated results for the Colpitts time series, synchronized as depicted in Figure 4. We observe that after an initial transient due to the initial condition mismatch both oscillators are synchronized. The Tx and Rx are shown in blue and orange, respectively. Next, we plot the error against time as illustrated in Figure 5, which shows that the coupling mechanism leads to perfect chaotic synchronization for an ideal channel. This is represented by a time series that stabilizes to zero after a transient period.

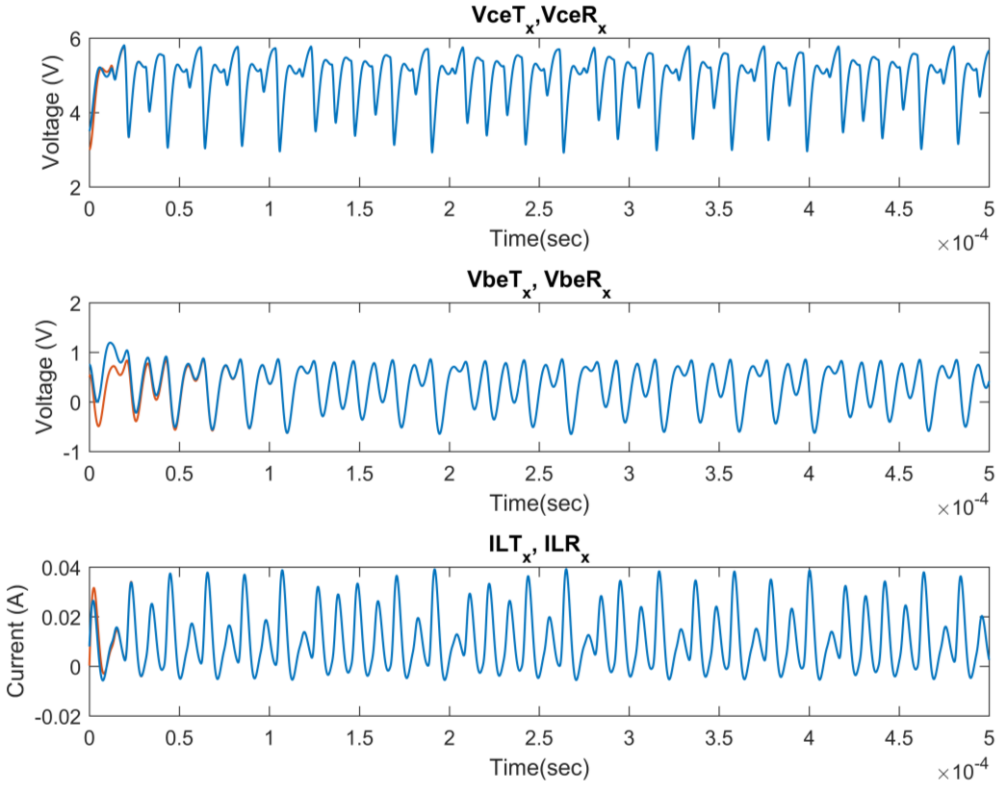

Figure 4. Colpitts time series synchronized.

Finally, we plot both attractors together as shown in Figure 6 and observe that both overlap after the initial transient.

The suggested coupling leads to a robust form of identical chaotic synchronization. We show in the following section that this is suitable for future implementations of chaotic inclusion techniques with Colpitts models in VLC links.

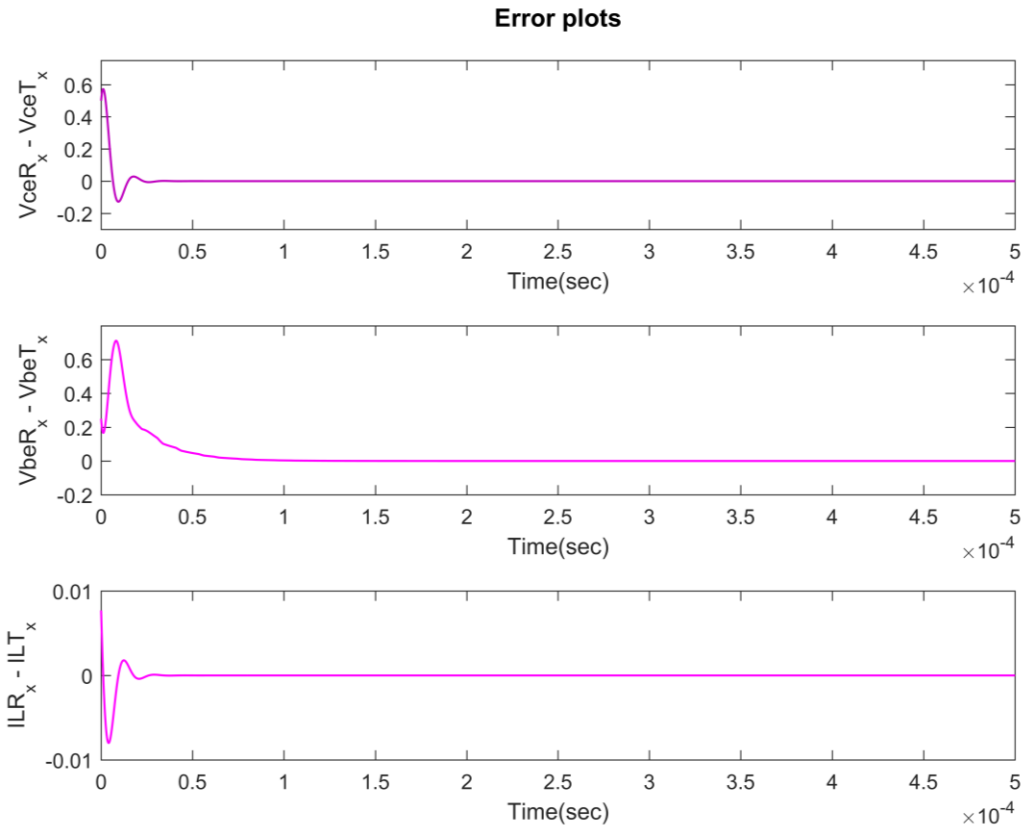

Figure 5. Error plots.

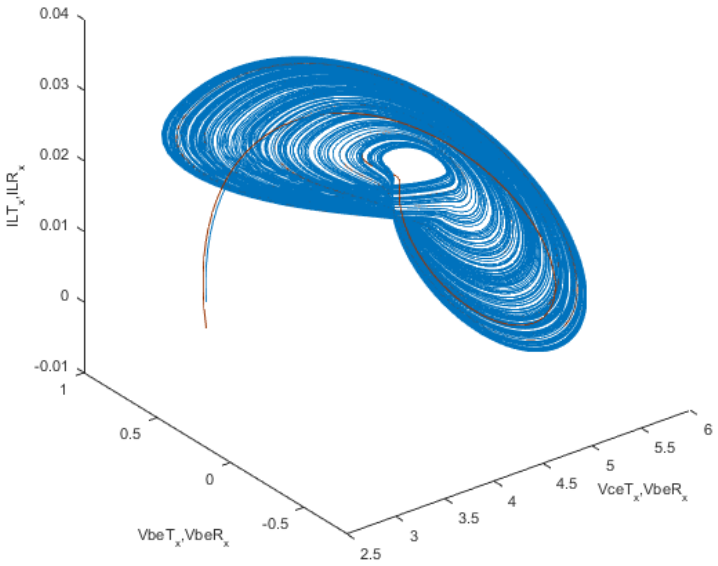

Figure 6. Colpitts attractors for Tx and Rx synchronized.

We finish this subsection with a brief discussion regarding the frequency of oscillation in chaotic models, in relation to time normalization mechanisms. Recalling that chaotic oscillators are composed of an infinite number of frequencies, it is tacitly admitted that a chaotic signal has a practical finite frequency bandwidth in which the most dominant frequency components are contained. Also, it is important to highlight that the frequency concept is borrowed from harmonic oscillation theory and that it does not neatly fit in the chaotic concept. The Colpitts chaotic bandwidth, for the model described in (1) and (2), is in the order of 100 kHz. One can see this by analyzing the spectral composition of

$V_{BE}(t)$. In order to increase this frequency, we apply a time normalization procedure. This consists in replacing d/dt with $d/d\tau$ where $\tau = t/T$, with T being the normalized time factor in the equation model. Then, with time normalization, the normalized frequency ω_{norm} can be gradually shifted from 100 kHz to the tens of MHz and above, allowing us to progressively observe the multipath effect on chaos synchronization. In the analog domain, the chaotic Colpitts time constant can be manipulated using the different discrete components to achieve higher frequencies (e.g., [30] for chaotic radar applications). Finally, since the model described in (1) and (2) is in continuous time; for numerical simulation purposes we employed a fixed step solver (Runge-Kutta, ode4) with a step size of $\Delta t = 10^{-7}$ s, which is scaled with T. This is effectively a discretization procedure from the analog to the digital domain.

2.2. VLC Multipath Channel Model

The model implemented consists of nine LED spot lights uniformly mounted on the ceiling of a $5 \times 5 \times 3$ m^3 (width, breadth, height) room as pictured in Figure 7. The LEDs are intensity modulated with the same chaotic carrier signal $V_{BE\_TX}(t)$. The Rxs are located 1 m above the floor level (simulating typical desk height) as it can be seen in Figure 8. Also shown in Figure 8 are both the LOS and non-LOS paths between LED and the Rx. Here only the first reflection (i.e., the most significant) is considered, which is ~7 dB (electrical) lower than the LOS component, and all subsequent reflections with little or no effect on the channel impulse response are ignored [31,32]. Note that the bandwidth of the white phosphorous LEDs, the most commonly deployed, is in the low MHz region (e.g., <5 MHz), and has a first order low-pass filter response [33], whereas the channel bandwidth in an indoor non-LOS transmission link is also limited by multipath propagation, resulting in inter-symbol interference (ISI). Indeed, the multipath induced fading, ISI, and resulting delay spread are one of the main challenges in chaos synchronization in VLC systems, and VLC systems in general. Here, we have assumed that the LED impulse response $h_{LED}(t)$ is ideal and there is no noise, to allow the study to focus on the multipath effect alone. This model replicates a common VLC experimental testbed employed for research purposes. This can be built using standard electronic components and driver boards at a relatively low cost. The chaotic signals used can be generated using digital signal processing means, facilitating its incorporation to already available VLC technology.

We investigate a MISO communication scheme where the Tx output is employed to drive a chaotic Rxs placed in three different floor positions, namely (0, 0), (2, 2), and (2.5, 2.5) considering the geometrical center to be the origin. The various positions of the Rxs determine the multipath delay induced, as we outline in the following.

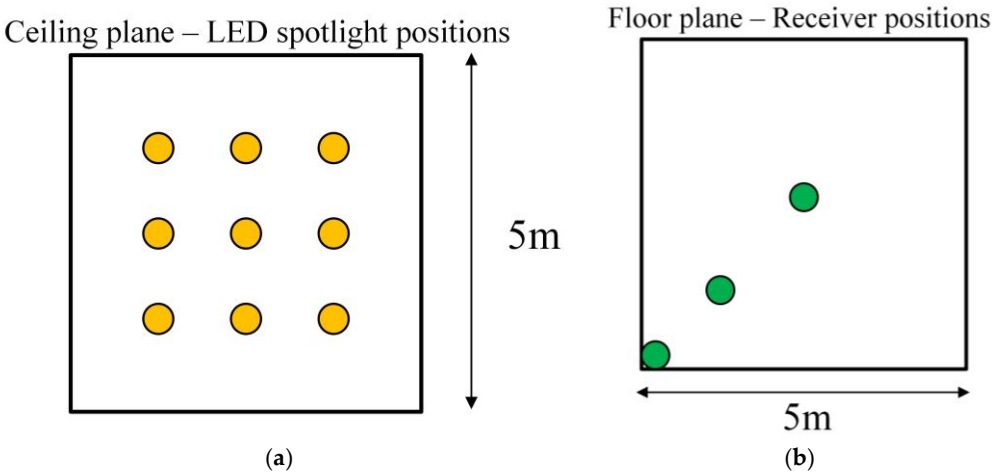

Figure 7. Typical room projections with Tx LED spotlights ceiling (**a**) and Rx positions (**b**).

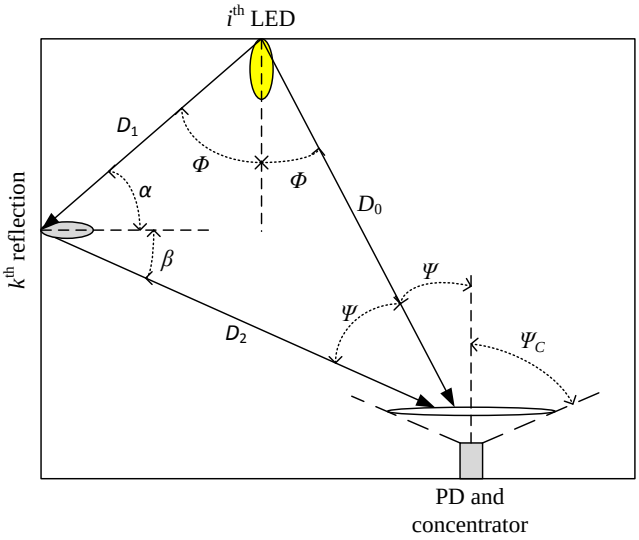

Figure 8. VLC with both LOS and non-LOS paths.

The channel impulse response in this model is given by:

$$h(t) = h_{LOS}(t) + h_{NLOS}(t), \tag{4}$$

where $h_{LOS}(t)$ and $h_{NLOS}(t)$ are the LOS and non-LOS impulse responses, respectively as defined in references [31,34]. Figure 9 shows the predicted impulse responses for three different Rx's positions of (0, 0), (2, 2), and (2.5, 2.5).

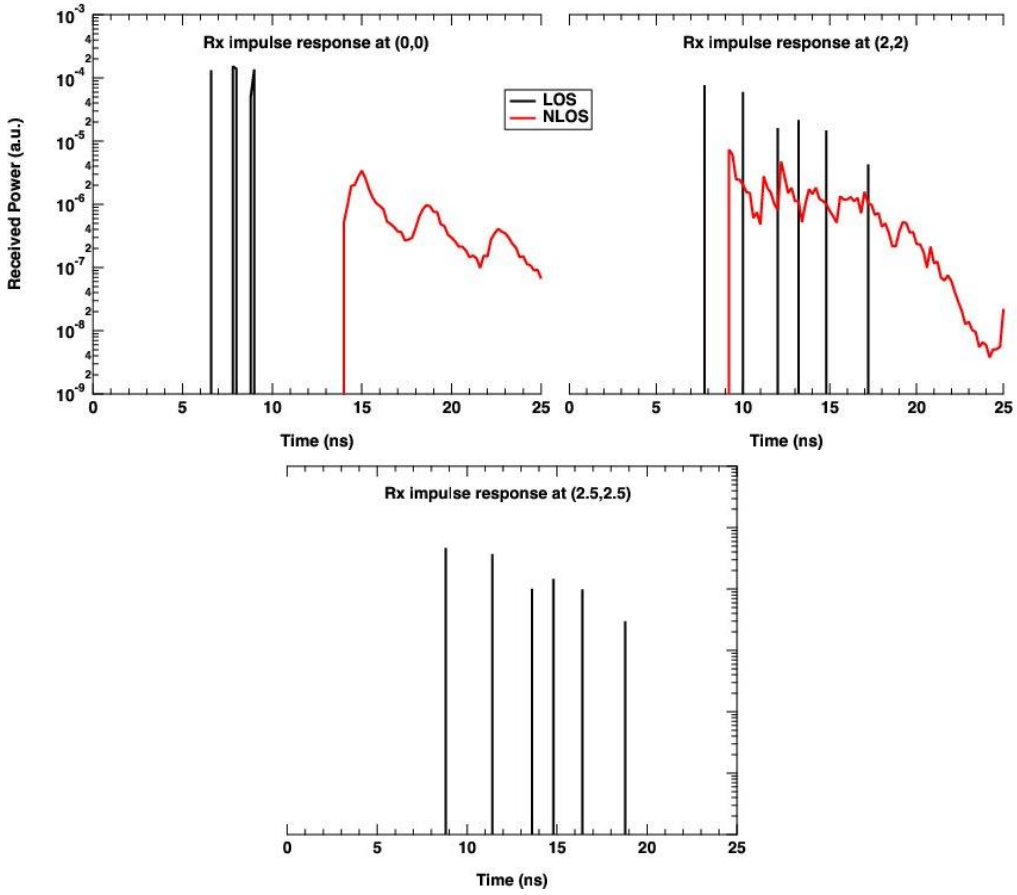

Figure 9. VLC with both LOS and non-LOS paths.

Based on the root mean square (RMS) delay spread analysis reported in [18], the average channel bandwidth is 100 MHz throughout the room. At the center of the room (i.e., position (0, 0)) there are 3 peaks for three different LOS paths (shortest to the longest), whereas at the position (2, 2), we observe responses from both LOS and non-LOS paths. Finally, with the Rx positioned at the corner of the room, lights arrive mostly from LOS paths with very little contributions from non-LOS paths.

3. Results

In this work, we study the influence of both $h_{LOS}(t)$ and $h_{NLOS}(t)$ on the chaotic carrier frequency by considering the Rx's positions, for which LOS is the dominant path. We show how this influence is due to the excess delay between the beams, which increases gradually with the carrier frequency of the chaotic signal; where this mean excess delay between each of the LOS paths being collected at the Rx becomes comparable to the period of the Tx signal. This is because all LED spotlights transmit the same signal, which when placing the Rx on the floor, we obtain LOS paths with the speed of the signal matching the delay spread more closely.

The proposed MISO system described in the previous section is numerically simulated. For this, the carrier's frequency is gradually increased in steps of 1 MHz until the cross-correlation coefficient is lower than 0.8—where it is considered that complete chaotic synchronization is lost. Accordingly, we steadily increased the frequency of the Colpitts carrier, establishing 12 scenarios, detailed in Table 1 with their corresponding correlation coefficient. For each scenario we have analyzed the correlation factor for each of the three Rx positions. Since the dimensions of the floor are squared (5 by 5 m), if we consider the geometrical center to be the coordinate (0, 0) testing the positions of the first quadrant (2, 2) and (2.5, 2.5) are equivalent for the remaining three quadrants due to the symmetry constraint.

Table 2 presents the correlation values for the chaotic carrier $V_{BE\_TX}(t)$ and its respective synchronized state $V_{BE\_RX}(t)$ for every corresponding position and frequency. This has been calculated using the standard cross-correlation equation between the transmitted signal and the corresponding generated signal for every position and the multipath model outlined in Section 2 given in [31,34].

Table 2. Correlation coefficients between $V_{BE\_TX}(t)$ and $V_{BE\_RX}(t)$.

Carrier Frequency	Position 1 (0, 0)	Position 2 (2, 2)	Position 3 (2.5, 2.5)
$T = 1$, $\omega = 100$ kHz	0.9987	0.9992	0.9992
$T = 30$, $\omega_{norm} = 3$ MHz	0.9814	0.9829	0.9848
$T = 40$, $\omega_{norm} = 4$ MHz	0.9721	0.9749	0.9749
$T = 50$, $\omega_{norm} = 5$ MHz	0.9577	0.9618	0.9669
$T = 60$, $\omega_{norm} = 6$ MHz	0.9373	0.9417	0.9480
$T = 70$, $\omega_{norm} = 7$ MHz	0.9183	0.9277	0.9371
$T = 80$, $\omega_{norm} = 8$ MHz	0.8985	0.9088	0.9192
$T = 90$, $\omega_{norm} = 9$ MHz	0.8770	0.8862	0.9106
$T = 100$, $\omega_{norm} = 10$ MHz	0.8703	0.8780	0.9000
$T = 110$, $\omega_{norm} = 11$ MHz	0.8275	0.8479	0.8701
$T = 120$, $\omega_{norm} = 12$ MHz	0.7986	0.8168	0.8440
$T = 130$, $\omega_{norm} = 13$ MHz	0.7510	0.7789	0.8050

Note that the scaling factor T is an arbitrary, proportional parameter with no units. Figure 10 shows the correlation values graphically against the normalized carrier frequency for the range of Rx's positions.

The correlation coefficient drops progressively as the carrier frequency is increased due to the multipath effect. In this case, synchronization is lost when the carrier frequency is higher than 12 MHz, where the correlation coefficient is in the order of 0.8.

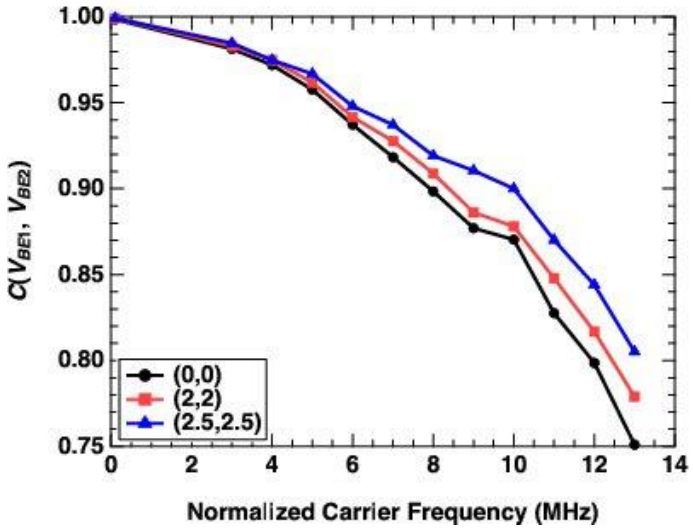

Figure 10. Cross correlation coefficients against normalized carrier frequency.

This study showed that the strongest impact on the synchronization quality is when the Rx is at the center of the room in contrast to the corners of the room where the correlation is higher. An explanation to this trend is because at the corners of the room the transmission mode is mostly LOS with very little non-LOS components. The last scenario is quite indicative of this tendency, where the correlation value in the corner of the room is above 0.8, which is considered the borderline. In contrast, correlation is in the order of 0.75 in the center. For $T = 1$, the correlation is almost 1 for all cases, showing that in the kHz region multipath effect has practically no impact.

4. Conclusions Discussion

In this work, we have presented a first chaos synchronization multipath effect study for VLC indoor applications. This approach can be used to provide data security at the physical layer in the context of VLC in compatibility with existing technology. For this we have employed discretized time-continuous chaotic models with time normalization procedures to progressively lift the chaotic carrier frequency. In addition, we have considered several receiver positions in the room floor. The multipath effect model considers the delays induced by LOS and non-LOS multipath fading in a MISO coupling scheme. The obtained results suggest that chaotic cryptosystems based on continuous-time chaotic models are feasible in VLC with an acceptable region operating beyond 10 MHz. This would be, at least for the Colpitts chaotic model and coupling, implemented as a testbed. We show that, as well as the chaotic carrier frequency, the Rx's position also influences chaotic synchronization. Results presented suggest that chaotic inclusion methods are feasible in VLC and reasonably robust against multipath effect delays.

Further research is to experimentally assess the performance of chaotic data transmission in a VLC setting employing the coupling method proposed in combination with a chaotic inclusion modulation method. Additionally, mutual synchronization methods could be developed from the research findings.

Author Contributions: P.C.-P. and P.A.H. equally contributed in conceiving and designing the study. A.B., H.L.-M. and Z.G. implemented the VLC multipath effect model employed. X.D. and T.T.S. and R.B. analyzed the data obtained in the context of communications and reviewed the work. Z.G. and K.B. supervised the research. P.C.-P. and P.A.H. wrote the paper.

Funding: This research was partly funded by EPSRC DTG grants EP/P505011/1, EP/P505623/1 and EP/J500276/1. This paper was also partly funded by the EPSRC grant EP/P006280/1: Multifunctional Polymer Light-Emitting Diodes with Visible Light Communications (MARVEL).

Acknowledgments: The authors acknowledge Northumbria University for supporting this research. The authors thank Claudio R. Mirasso from the Institute for Cross Disciplinary Physics and Complex Systems (IFISC) at the University of the Balearic Islands (Spain) for fruitful discussions and relevant feedback.

Conflicts of Interest: The authors declare no conflict of interest.

References

1. Kocarev, L.; Lian, S. *Chaos-Based Cryptography: Theory, Algorithms and Applications*; Springer: Berlin, Germany, 2011; ISBN 9783662506530.
2. Pecora, L.M.; Carroll, T.L. Synchronization of chaotic systems. *Chaos* **2015**, *25*, 097611. [CrossRef] [PubMed]
3. Boccaletti, S.; Kurths, J.; Osipov, G.; Valladares, D.L.; Zhou, C.S. The synchronization of chaotic systems. *Phys. Rep.* **2002**, *366*, 1–101. [CrossRef]
4. Alvarez, G.; Li, S. Some basic cryptographic requirements for chaos-based crypto systems. *Int. J. Bifurc. Chaos* **2006**, *16*, 2129–2151. [CrossRef]
5. Le Minh, H.; O'Brien, D.; Faulkner, G.; Zeng, L.; Lee, K.; Jung, D.; Oh, Y.J. High-speed visible light communications using multiple-resonant equalization. *IEEE Photonics Technol. Lett.* **2008**, *20*, 1243–1245. [CrossRef]
6. Grobe, L.; Paraskevopoulos, A.; Hilt, J.; Schulz, D.; Lassak, F.; Hartlieb, F.; Kotte, C.; Jungnickel, V.; Langer, K.D. High-speed Visible Light Communication Systems. *IEEE Commun. Mag.* **2013**, *51*, 60–66. [CrossRef]
7. Jovicic, A.; Li, J.; Richardson, T. Visible light communication: Opportunities, challenges and the path to market. *IEEE Commun. Mag.* **2013**, *51*, 26–32. [CrossRef]
8. Wu, S.; Wang, H.; Youn, C.H. Visible light communications for 5G wireless networking systems: From fixed to mobile communications. *IEEE Netw.* **2014**, *28*, 41–45. [CrossRef]
9. Tsiropoulou, E.E.; Gialagkolidis, I.; Vamvakas, P.; Papavassiliou, S. Resource allocation in visible light communication networks: NOMA vs. OFDMA transmission techniques. In Proceedings of the International Conference on Ad-Hoc Networks and Wireless, Lille, France, 4–6 July 2016; Springer: Cham, Switzerland, 2016; pp. 32–46.
10. Singhal, C.; De, S. (Eds.) *Resource Allocation in Next-Generation Broadband Wireless Access Networks*; IGI Global: Hershey, PA, USA, 2017.
11. Bykhovsky, D.; Arnon, S. Multiple access resource allocation in visible light communication systems. *J. Lightw. Technol.* **2014**, *32*, 1594–1600. [CrossRef]
12. Chen, Z.; Tsonev, D.; Haas, H. Improving SINR in indoor cellular visible light communication networks. In Proceedings of the IEEE International Conference on Communications (ICC), Sydney, Australia, 10–14 June 2014.
13. IEEE Standard Association. *IEEE Standard for Local and Metropolitan Area Networks—Part 15.7: Short-Rang Wireless Optical Communication Using Visible Light*; IEEE Computer Society: Wahington, DC, USA, 2011.
14. Chaleshtori, Z.N.; Chvojka, P.; Zvanovec, S.; Ghassemlooy, Z.; Haigh, P.A. A Survey on Recent Advances in Organic Visible Light Communications. In Proceedings of the IEEE 11th International Symposium on Communication Systems, Networks & Digital Signal Processing (CSNDSP), Budapest, Hungary, 18–20 July 2018.
15. Bates, R.; Geldard, C.; Hassan, N.B.; Burton, A.; Luo, P. Comparison of LED illumination patterns for camera based car to car communications. In Proceedings of the 10th International Symposium on Communication Systems, Networks and Digital Signal Processing (CSNDSP), Prague, Czech Republic, 20–22 July 2016.
16. Chen, C.W.; Wang, W.C.; Wu, J.T.; Chen, H.Y.; Liang, K.; Wei, L.Y.; Hsu, Y.H.; Chow, C.W.; Yeh, C.H.; Liu, Y.; et al. Visible light communications for the implementation of internet-of-things. *Opt. Eng.* **2016**, *55*, 060501. [CrossRef]
17. Burton, A.; Le Minh, H.; Ghassemlooy, Z.; Rajbhandari, S.; Haigh, P.A. Smart receiver for visible light communications: Design and Analysis. In Proceedings of the 8th International Symposium on Communication Systems, Networks and Digital Signal Processing (CSNDSP), Poznan, Poland, 18–20 July 2012.
18. Burton, A.; Ghassemlooy, Z.; Rajbhandari, S.; Liaw, S.K. Design and analysis of an angular-segmented full-mobility visible light communications receiver. *Trans. Emerg. Telecommun. Technol.* **2014**, *25*, 591–599. [CrossRef]

19. Aguado, A.; Hugues-Salas, E.; Haigh, P.A.; Marhuenda, J.; Price, A.B.; Sibson, P.; Kennard, J.; Erven, C.; Rarity, J.G.; Thompson, M.G.; et al. First Experimental Demonstration of Secure NFV Orchestration over an SDN-Controlled Optical Network with Time-Shared Quantum Key Distribution Resources. In Proceedings of the 42nd European Conference on Optical Communication (ECOC), Düsseldorf, Germany, 18–22 September 2016.
20. Jouguet, P.; Kunz-Jacques, S.; Leverrier, A.; Grangier, P.; Diamanti, E. Experimental demonstration of long-distance continuous-variable quantum key distribution. *Nat. Photonics* **2013**, *5*, 378–381. [CrossRef]
21. Stinson, D.R. *Cryptography: Theory and Practice*; Chapman & Hall/CRC: Boca Raton, FL, USA, 2006; ISBN 9781584885085.
22. Álvarez, G.; Li, S.; Montoya, F.; Pastor, G.; Romera, M. Breaking projective chaos synchronization secure communication using filtering and generalized synchronization. *Chaos Solitons Fractals* **2005**, *24*, 775–783. [CrossRef]
23. Li, S.; Álvarez, G.; Chen, G. Breaking a chaos-based secure communication scheme designed by an improved modulation method. *Chaos Solitons Fractals* **2005**, *25*, 109–120. [CrossRef]
24. Millerioux, G.; Amigó, J.M.; Daafouz, J. A Connection Between Chaotic and Conventional Cryptography. *IEEE Trans. Circuits Syst. I Reg. Pap.* **2008**, *55*, 1695–1703. [CrossRef]
25. Ren, H.P.; Baptista, M.S.; Grebogi, C. Wireless communication with chaos. *Phys. Rev. Lett.* **2013**, *110*, 184101. [CrossRef] [PubMed]
26. Ren, H.P.; Bai, C.; Baptista, M.S.; Greborgi, C. Experimental validation of wireless communication with chaos. *Chaos* **2016**, *26*, 083117. [CrossRef] [PubMed]
27. Kennedy, M.P. Chaos in the Colpitts oscillator. *IEEE Trans. Circuits Syst. I Fundam. Theory Appl.* **1994**, *41*, 771–774. [CrossRef]
28. Uchida, A.; Kawano, M.; Yoshimori, S. Dual synchronization of chaos in Colpitts electronic oscillators and its applications for communications. *Phys. Rev. E* **2003**, *68*, 056207. [CrossRef] [PubMed]
29. Rubezic, V.; Ostojic, R. Synchronization of chaotic Colpitts oscillators with applications to binary communications. In Proceedings of the 6th IEEE International Conference on Electronics, Circuits and Systems (ICECS), Pafos, Cyprus, 5–8 September 1999.
30. Beal, A.; Blakely, J.N.; Corron, N.J.; Dean, R.N. High frequency oscillators for chaotic radar. In Proceedings of the SPIE Radar Sensor Technology, Baltimore, MD, USA, 18–21 April 2016.
31. Ghassemlooy, Z.; Popoola, W.O.; Rajbhandari, S. *Optical Wireless Communications: System and Channel Modelling with MATLAB*; CRC Press, Taylor and Francis Group: Boca Raton, FL, USA, 8 August 2012; ISBN 9781138074804.
32. Zeng, L.; O'Brien, D.; Le Minh, H.; Faulkner, G.E.; Lee, K.; Jung, D.; Oh, Y.J.; Won, E.T. High data rate multiple input multiple output (MIMO) optical wireless communications using white LED lighting. *IEEE J. Sel. Areas Commun.* **2009**, *27*, 1654–1662. [CrossRef]
33. Haigh, P.A.; Ghassemlooy, Z.; Rajbhandari, S.; Papakonstantinou, I.; Popoola, W. Visible Light Communications: 170 Mb/s Using an Artificial Neural Network Equalizer in a Low Bandwidth White Light Configuration. *J. Lightw. Technol.* **2014**, *32*, 1807–1813. [CrossRef]
34. Burton, A.; Le Minh, H.; Ghassemlooy, Z.; Rajbhandari, S. A study of LED lumination uniformity with mobility for visible light communications. In Proceedings of the International Workshop on Optical Wireless Communications (IWOW), Newcastle-upon-Tyne, UK, 22 October 2012.